Long-term tidal evolution of the TRAPPIST-1 system

Brasser, R.; Pichierri, G.; Dobos, V.; Barr, A. C.

IMPORTANT NOTE: You are advised to consult the publisher's version (publisher's PDF) if you wish to cite from it. Please check the document version below.

Document Version
Publisher's PDF, also known as Version of record

[Link to publication in University of Groningen/UMCG research database](#)

Long-term tidal evolution of the TRAPPIST-1 system

R. Brasser,[1]★ G. Pichierri [®],[2] V. Dobos[3,4] and A. C. Barr[5]

[1]*Origins Research Institute, Research Centre for Astronomy and Earth Sciences, MTA Centre of Excellence, Konkoly Thege Miklos St 15-17, H-1121 Budapest, Hungary*
[2]*Max Planck Institute for Astronomy, Köningstuhl 17, D-69117 Heidelberg, Germany*
[3]*Kapteyn Astronomical Institute, University of Groningen, Landleven 12, NL-9747 AD Groningen, the Netherlands*
[4]*MTA-ELTE Exoplanet Research Group, H-9700, Szent Imre h. u. 112, Szombathely, Hungary*
[5]*Planetary Science Institute, 1700 East Fort Lowell, Suite 106, 85719 Tucson AZ, USA*

ABSTRACT

The ultracool M-dwarf star TRAPPIST-1 is surrounded by seven planets configured in a resonant chain. Transit-timing variations have shown that the planets are caught in multiple three-body resonances and that their orbits are slightly eccentric, probably caused by resonant forcing. The current values of the eccentricities could be a remnant from their formation. Here, we run numerical simulations using fictitious forces of trapping the fully grown planets in resonances as they migrated in the gas disc, followed by numerical simulations detailing their tidal evolution. For a reduced disc scale height $h \sim 0.03$–0.05, the eccentricities of the planets upon capture in resonance are higher than their current values by factors of a few. We show that the current eccentricities and spacing of planets d to h are natural outcomes of coupled tidal evolution wherein the planets simultaneously damp their eccentricities and separate due to their resonant interaction. We further show that the planets evolve along a set of equilibrium curves in semimajor axis–eccentricity phase space that are defined by the resonances, and that conserve angular momentum. As such, the current $8{:}5$–$5{:}3$–$(3{:}2)^2$–$4{:}3$–$3{:}2$ resonant configuration cannot be reproduced from a primordial $(3{:}2)^4$–$4{:}3$–$3{:}2$ resonant configuration from tidal dissipation in the planets alone. We use our simulations to constrain the long-term tidal parameters k_2/Q for planets b to e, which are in the range of 10^{-3} to 10^{-2}, and show that these are mostly consistent with those obtained from interior modelling following reasonable assumptions.

Key words: methods: numerical – planets and satellites:: dynamical evolution and stability – planets and satellites: fundamental parameters – planets and satellites: terrestrial planets.

1 INTRODUCTION

The star TRAPPIST-1 is an ultracool M-dwarf that harbours seven roughly Earth-sized planets (Gillon et al. 2017). All of these planets orbit within 0.07 au of the star, and have orbital periods from 1.5 d to ∼19 d (Gillon et al. 2017; Grimm et al. 2018; Agol et al. 2021). The planets are in a resonant chain, possibly involving all the planets, which results in the libration of a number of three-body resonant angles (Luger et al. 2017). The orbits of all planets appear to be mildly eccentric, with eccentricities ≲0.01, although the orbits of the two inner planets could be circular (Agol et al. 2021). The eccentricities are possibly the result of forcing from the resonances or a remnant of their formation. Each of the planets has a density intermediate between the densities of compressed water ice and the Earth's inner core (Gillon et al. 2017; Barr, Dobos & Kiss 2018; Grimm et al. 2018; Agol et al. 2021), implying solid planets composed of rock, metal (Elkins-Tanton & Seager 2008), and possibly ice if atmospheric conditions allow (Turbet et al. 2020, see Fig. 1). With recent estimates for the planetary masses the system appears dynamically stable on Myr, and possibly Gyr time-scales (Grimm et al. 2018; Agol et al. 2021).

There is much uncertainty about the formation of the system, which is an active topic of research. Based on dynamical simulations, Tamayo et al. (2017) suggested that the current resonant structure was the result of convergent migration within the primordial gas disc. That same year Ormel, Liu & Schoonenberg (2017) suggested that the system could have been formed through a combination of planet migration and pebble accretion. More recently Huang & Ormel (2022) expanded on the pebble accretion idea with the addition of specific requirements for the interior structure of the disc and the configuration of the planets.

Short-term (≲1 Myr) numerical simulations indicate that for many initial conditions within the observational uncertainties almost all of the resonant angles appear to librate (Grimm et al. 2018; Brasser, Barr & Dobos 2019; Agol et al. 2021). Their long-term (>1 Gyr) stability cannot be determined with the current observational uncertainties (Agol et al. 2021). From older observational data with larger uncertainties Brasser et al. (2019) found that most three-body resonances break on short time-scales (<1 Myr).

It is not clear whether the inner two planets, b and c, are truly involved in mean-motion resonances. Planets b and c are close to a mutual 8:5, and c and d in a 5:3 resonance (Gillon et al. 2017; Luger et al. 2017). This configuration warrants attention because the outer five planets all reside in first-order mean motion resonances; these two resonances are of second and third order, respectively. Indeed,

★ E-mail: ramon.brasser@csfk.org
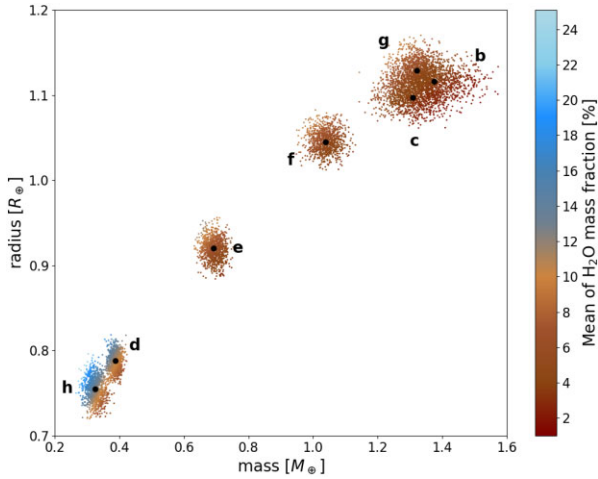
Figure 1. H_2O content (indicated by colours) for possible interior structures at a given mass–radius pair of the TRAPPIST-1 planets. The mean of the H_2O mass fraction is presented (including liquid water, ice I, and high-pressure ice polymorphs) for all possible interior structures calculated for each mass–radius pairs. The calculation method used is the same as described in the work of Dobos, Barr & Kiss (2019) with the additional condition that only those interior structures were considered that contain 10–50 per cent mass fraction of iron core. Masses and radii are from Agol et al. (2021) with black dots denoting the mean values.

Teyssandier, Libert & Agol (2022) showed that convergent migration in the gas disc leads to capture primarily in first-order mean-motion resonances, and that the 8:5 resonance between planets b and c, as well as the 5:3 between planets c and d, are difficult to explain via this mechanism. In this work, we explore whether the current configuration can be obtained by tidal dissipation in the planets from an initial configuration consisting only of first-order mean-motion resonances because such a configuration is the expected outcome from planet migration. In the subsection below this is explained in more detail.

1.1 Basic outline of resonant trapping

The formation of the TRAPPIST-1 planets is not yet well understood, but recent studies point to a potential combination of pebble accretion and planet migration (Ormel et al. 2017; Unterborn et al. 2018; Schoonenberg et al. 2019) possibly followed by rebound because of the dispersion of the disc as well as tidal dissipation in the planets (Huang & Ormel 2022). An alternative scenario relies on different modes of migration (Ogihara et al. 2022). As the planets migrate through the disc towards the star they will encounter mutual mean-motion resonances (e.g. Petrovich, Malhotra & Tremaine 2013); this is especially so if the innermost planet stalls at the inner edge of the disc and the subsequent planet migrate towards it (e.g. Ogihara, Duncan & Ida 2010).

The current configuration of the planets is in a suspected 8:5–5:3–(3:2)^2–4:3–3:2 resonant chain (Gillon et al. 2017; Luger et al. 2017), which can be obtained through planet migration (Tamayo et al. 2017). Yet other simulations of the formation of the system preferentially show trapping in a different configuration, e.g. (3:2)^4–4:3–3:2 (Huang & Ormel 2022; Teyssandier et al. 2022). Here, we briefly describe how resonant trapping works and why the latter configuration is more likely than the former.

Away from resonances, the averaged disturbing function that describes the orbital evolution of two planets is the secular part,

which is given by (Murray & Dermott 1999)

$$\mathcal{R}_D^{sec} = \tfrac{1}{8}\alpha b_{3/2}^{(1)}(\alpha)\left(e^2 + e'^2\right) - \tfrac{1}{4}\alpha b_{3/2}^{(1)}(\alpha)ee'\cos(\varpi - \varpi'), \quad (1)$$

where e and e' are the eccentricities of the inner and outer planet, ϖ and ϖ' are their longitudes of periastron, $\alpha = a/a'$ is the ratio of semimajor axes, and $b_s^{(j)}(\alpha)$ are the so-called Laplace coefficients, which can be expressed in terms of Gamma and hypergeometric functions (Murray & Dermott 1999). In a two-or-more-planet system each planet has a free eccentricity and a forced eccentricity caused by their mutual perturbations. The motion of the eccentricities and longitudes of perihelia of a two-planet system are coupled via

$$e_1 \exp(\iota\varpi_1) = M_{1,1}\exp[\iota(g_1 t + \beta_1)] + M_{1,2}\exp[\iota(g_2 t + \beta_2)],$$
$$e_2 \exp(\iota\varpi_2) = M_{2,1}\exp[\iota(g_1 t + \beta_1)] + M_{2,2}\exp[\iota(g_2 t + \beta_2)]. \quad (2)$$

The $M_{i,i}$ terms are the free eccentricities, while the $M_{i,j}$ terms are the forced eccentricities, and t is the time. The frequencies g_i are the eccentricity eigenfrequencies with their corresponding phases β_i, and $\iota^2 = -1$ is the imaginary unit.

Near a mean-motion resonance the angles of the form $\phi = j_1\lambda + j_2\lambda' + j_3\varpi + j_4\varpi'$, where $j_1, \ldots, j_4$ are integers, will vary slowly, on time-scales much longer than the orbital periods of the planets, and cannot be eliminated from the problem through averaging. The angle ϕ satisfies the D'Alembert rule that $\sum_i j_i = 0$.

When planets are in a mean-motion resonance the resonant disturbing function will typically be of the form (Murray & Dermott 1999)

$$\mathcal{R} = \mathcal{R}_D^{sec} + e^{|j_3|}e'^{|j_4|}(f_d(\alpha) + f_e(\alpha)\cos\phi), \quad (3)$$

where $f_d(\alpha)$ and $f_e(\alpha)$ are functions of Laplace coefficients. It is immediately obvious that the strength of the resonant perturbation depends on the product $e^{|j_3|}e'^{|j_4|}$ i.e. on $j_3 + j_4$, which itself depends on $j_1 + j_2$. For a first-order resonance, such as the 2:1, the 3:2, or the 4:3, we have $|j_1 + j_2| = 1$ and thus $|j_3 + j_4| = 1$, and $\mathcal{R} \propto e$ or $\mathcal{R} \propto e'$. For a second-order resonance, such as the 3:1 or the 5:3, we have $|j_1 + j_2| = 2$, so that by necessity $|j_3 + j_4| = 2$ and either $\mathcal{R} \propto e^2$, or $\mathcal{R} \propto ee'$, or $\mathcal{R} \propto e'^2$. For a third-order resonance, such as the 4:1 or the 8:5, $\mathcal{R}$ is proportional to the third power in the eccentricities, and so forth. A resonant pair of planets will have non-zero forced eccentricities if they are in equilibrium.

The interaction of the planets with the gas disc causes them to migrate towards the star and to have their free eccentricities damped (Tanaka & Ward 2004) i.e. the $M_{i,i}$ terms will approach zero – and by necessity so will the $M_{i,j}$ terms because they depend indirectly on the $M_{i,i}$ terms. In essence, the planets approach the mean-motion resonance with (close to) zero free eccentricities. For low eccentricities the perturbations from first-order resonances will far exceed those from second- or third-order resonances due to the argument $e^{|j_3|}e'^{|j_4|}$ in the disturbing function. Capture in (first-order) resonance is facilitated by lower eccentricities (Henrard 1982), so that the *expectation* is that the planets will be trapped into *first-order* mean-motion resonances when they are migrating starwards, rather than into higher order resonances.

Once the planets are captured into first-order mean-motion resonances while they are migrating, each pair of planets will approach the resonance with a period ratio greater than the exact resonant value, and their eccentricities will increase due to the increasing importance of the resonant perturbations over the secular perturbations. The resulting eccentricities are forced eccentricities. The planets will reach an equilibrium between the eccentricity pumping from the resonance and the damping of the gas disc, with the equilibrium eccentricity being approximately $e \sim 1.3h$ (Goldreich & Schlichting
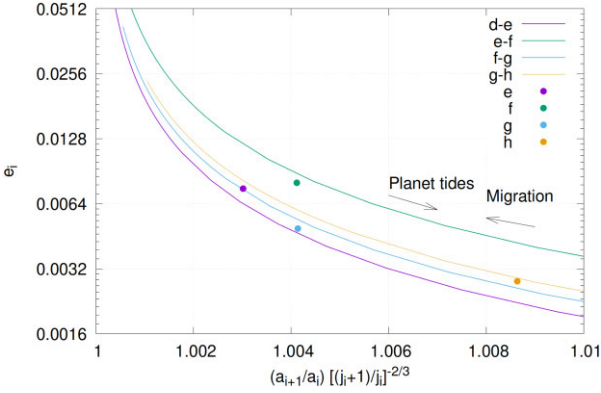
Figure 2. Normalized resonant loci of several resonances in the TRAPPIST-1 system. The dots show the current configuration of the system. Arrows indicate the direction of motion along the lines for disc-induced migration, and for tidal dissipation in the planets.

2014; Pichierri, Morbidelli & Crida 2018; Brasser et al. 2019) where h is the reduced scale height of the gas disc.

What we currently observe is that the outer five planets are in a 3:2–3:2–4:3–3:2 chain (Luger et al. 2017) with eccentricities below 0.01, but the inner three are in a potential 8:5–5:3 chain (Luger et al. 2017), which is of third and second order respectively. The probability of capturing the planets in these higher order resonances during the migration phase is very low (Papaloizou, Szuszkiewicz & Terquem 2018). Tamayo et al. (2017) were able to migrate all seven planets into the current resonant chain by starting the planets a few per cent wide of their current resonances and only applying migration torques to planet h. In contrast, Huang & Ormel (2022) advocate a primordial $(3:2)^4$–4:3–3:2 configuration that was disrupted by rebound from the dispersing gas disc followed by tidal dissipation in the planets. In the next section, we introduce a resonant model for such a chain which encapsulates the main dynamical effects of planetary migration and planetary tides on the planets.

1.2 Resonant loci for a TRAPPIST-1 $(3:2)^4$–4:3–3:2 chain

The evolution of the system is readily derived from the parametrization shown in Fig. 2. All planet pairs will evolve along equilibrium lines that are determined by the Hamiltonian of the system. The resonant Hamiltonian model for any resonance or resonant chain can be constructed following the recipe presented in Batygin & Morbidelli (2013b) for two planets, and extended to the multiple-planet case. For example, the framework presented in Pichierri, Batygin & Morbidelli (2019) applies to three resonant planets; this procedure is extended here to encompass the seven-planet case of TRAPPIST-1. Even when the Hamiltonian is expanded to first order in the eccentricities – which is justified by the low eccentricities of the TRAPPIST-1 planets – the resulting Hamiltonian is not integrable when there are more than two planets, and the resonant equilibria cannot be found analytically. As such, one has to resort to numerical optimization methods to obtain the location of the equilibria of the resonant system, which we call resonant equilibrium points. We implemented the resulting semi-analytical scheme in the `Mathematica` language and used the `FindRoot` function to find the extrema of the Hamiltonian.[1]

---

[1]We note that we included only interactions between neighbouring planets in the resonant model. Given the large number of variables [there are $2(N_{pl}$

Since the problem is scale free, let us think in terms of semimajor-axis ratios between the planets; this is equivalent to having fixed units of length such that the nominal resonant location of planet b is e.g. $a_{b, res} = a_{b, obs}$, i.e. its currently observed value. For a fixed value of the total angular momentum of the system one can find one stable resonant locus, which then determines the semimajor axes and eccentricities of all planets relative to each other via the equilibrium resonant condition. By varying the value of the total angular momentum, one gets a whole family of equilibrium points, parametrized by the angular momentum of the system (or, equivalently, by any one of the eccentricities or semimajor axes of a specific TRAPPIST-1 planet).

Such scale-free equilibrium curves are displayed in Fig. 2 on a plane with $(a_{i+1}/a_i) \times [(j_i + 1)/j_i]^{-2/3}$ on the horizontal axis versus the eccentricity e_i on the vertical axis (i being a label for each pair of subsequent planets along the chain), for the four outermost planets. Here, j_i are the indices of the $(j_i + 1)$: j_i mean-motion resonances along the $(3:2)^4$–4:3–3:2 chain, namely $j_1 = j_2 = j_3 = j_4 = j_6 = 2$ and $j_5 = 3$. The main feature to note of these curves is that at decreasing eccentricities the resonant loci deviate away from the exact commensurability $(a_{i+1}/a_i) \times [(j_i + 1)/j_i]^{-2/3} = 1$; this effect is well known (e.g. Delisle et al. 2012; Pichierri et al. 2019) and is due to the faster precession of the pericentres at vanishing e because to first order $\varpi \propto e^{-1}$. The resonant locus for a single-planet pair is linked to corresponding loci for all other planet pairs by the total angular momentum of the system. Therefore, in a resonant chain, lowering the eccentricity of one planet along the curve forces all other eccentricities to decrease as well. The dots show the current normalized semimajor axial ratio and eccentricities of planets e to h. Migration induced by disc torques will cause each planet to move leftwards along the equilibrium lines while planetary tides will cause them to move in the opposite direction (Delisle et al. 2012; Pichierri et al. 2019).

Here, we investigate the tidal evolution of the system starting from both the current resonant chain and a $(3:2)^4$–4:3–3:2 configuration with the aim to constrain the tidal parameters in some of the inner four planets. We further aim to establish whether the current state can be reproduced through tidal dissipation in the planets from a primordial $(3:2)^4$–4:3–3:2 configuration. This problem was partially studied by Papaloizou et al. (2018), but they used old values for the planetary masses and radii. Here, we make use of the latest masses and radii from Agol et al. (2021).

2 METHODOLOGY

2.1 Resonant trapping

The first step in our analysis of possible past and present resonant states for the TRAPPIST-1 planets requires the build-up of a resonant chain. Tamayo et al. (2017) showed that a TRAPPIST-1 system with period ratios close to the current observed ones can be obtained by implementing inward migration applied only to the outermost planet

---

$- 1)$ degrees of freedom in a resonant chain of N_{pl} planets, therefore $4(N_{pl} - 1) = 24$ variables for the full TRAPPIST-1 chain], this approach becomes numerically more feasible since the stable equilibria we are interested in only occur for values of the resonant arguments equal to 0 or π, thus cutting by half the number of equations to be solved numerically. This approach does not consider the 2:1 contribution between planets e and g, which would shift the loci only slightly in the semimajor-axial ratio v.s. e space, without however changing the main feature of the resonant curves used in this paper.

TRAPPIST-1h, thus hinting to a dynamical past marked by planet–disc interactions reminiscent of type-I migration. We should keep in mind that this approach to explain the precise formation history of the system is probably too simplistic, since migration should be applied to all planets at once, which, given their non-uniformity in planetary mass along the chain, would actually result in both convergent and divergent migration for specific planet pairs. Indeed, more sophisticated formation histories seem to be necessary to form an initial resonant state close to the current one (e.g. Huang & Ormel 2022). For the purposes of our analysis, however, we make use of a recipe similar to that proposed by Tamayo et al. (2017) only so that we can reliably form a desired chain, in order to then study its long-term tidal evolution after gas disc dissipation. Indeed, the advantage of the approach of Tamayo et al. (2017) is that migration only involves planets that have already assumed a resonant relationship with planets farther out, which makes the process more controllable. It also allows the innermost planets to be captured in the high-order 8:5 and 5:3 resonances, even if one would actually expect first-order resonances to be favoured as explained in the Introduction. This trapping behaviour can be observed in the work of Teyssandier et al. (e.g. 2022) and is confirmed by our own simulations of the innermost three- and four-planet system under conventional type-I migration prescriptions obtained from Cresswell & Nelson (2008). The trapping in the higher order resonances is facilitated because the planets approach these higher order resonances with already non-zero eccentricities induced by their resonant interactions with planets farther out.

For our migration simulations we used the *N*-body integrator SyMBA (Duncan, Levison & Lee 1998), which was modified to include the forces from a gas disc and migration, as detailed below. We consider type-I inward migration applied to planet h only, with a migration time-scale taken from Cresswell & Nelson (2008) in the planar case:

$$\tau_{\mathrm{mig}} = 2\frac{\tau_{\mathrm{wave}}}{(2.7 + 1.1\alpha_\Sigma)}h^{-2}\left(P(e) + \frac{P(e)}{|P(e)|}\right),\tag{4}$$

where

$$P(e) = \frac{1 + \left(\frac{e}{2.25h}\right)^{1/2} + \left(\frac{e}{2.84h}\right)^6}{1 - \left(\frac{e}{2.02h}\right)^4}.\tag{5}$$

We instead apply eccentricity damping to all planets, following the formula from Cresswell & Nelson (2008) in the planar case:

$$\tau_e = \frac{\tau_{\mathrm{wave}}}{0.780}\left[1 - 0.14\left(\frac{e}{h}\right)^2 + 0.06\left(\frac{e}{h}\right)^3\right].\tag{6}$$

In these formulae $h = H/r$ is the reduced scale height of the disc, and τ_{wave} is the wave time-scale given by (Tanaka & Ward 2004)

$$\tau_{\mathrm{wave}} = \left(\frac{M_*}{m_{\mathrm{pl}}}\right)\left(\frac{M_*}{\Sigma_{\mathrm{gas,pl}}a_{\mathrm{pl}}^2}\right)h_{\mathrm{pl}}^4\Omega_{K,\mathrm{pl}}^{-1},\tag{7}$$

where m_{pl} is the mass of the planet, M_* that of the star, and $\Omega_{K,\mathrm{pl}}$ is the frequency of Keplerian motion, and all quantities with the label 'pl' are evaluated at the location of the planet. We used aspect ratios values of $h = 0.04$ and $h = 0.05$, which has the effect of obtaining slightly different capture eccentricities, since $e_{\mathrm{capt.}} \approx \sqrt{\tau_e/\tau_a} \approx 1.3h$ (Goldreich & Schlichting 2014; Pichierri et al. 2018, see also Section 1.1). The same formula shows that τ_{wave} does not influence the final captured state, and thus neither does the surface density $\Sigma_{\mathrm{gas,pl}}$, provided that migration is slow enough to allow for adiabatic resonant capture. The masses of the individual planets used in this simulation are 1.43, 1.34, 0.37, 0.68, 1.02, 1.29, and 0.31 $M_\oplus$.

2.2 SWIFT MVS frequency map analysis

After trapping the planets into a resonant chain we need to establish how close the planets are to actual resonances. It is not sufficient to look at the evolution of the semimajor axes or the resonant angles, because the latter can still librate far from resonance if the system is tidally evolved (Delisle et al. 2012; Batygin & Morbidelli 2013a). In most *N*-body codes, such as SWIFT MVS (Mixed Variable Symplectic) (Levison & Duncan 1994) or *Mercury* (Chambers 1999), the semimajor axis output are osculating values that depend on the relative positions of the planets to each other. These osculating values will not yield high-precision orbital frequencies without filtering. As such, we have taken a different approach and implemented direct Fourier analysis in the *N*-body symplectic integrator SWIFT MVS (Levison & Duncan 1994) as follows.

During the simulations the *x* and *y* co-ordinates of the planets are stored in arrays, which are thinned by a factor of four to conserve memory. The MVS method relies on the symplectic mapping of Wisdom & Holman (1991), which requires at least 20 steps per orbit to preserve accuracy. Our thinning therefore leaves at least five coordinate values for the orbit of the innermost planet which, through experimentation, we have determined to be enough to ensure an accurate computation of the orbital frequency. The size of the arrays is an input parameter, which needs to be equal to a power of two, and which has a current maximum dimension of 262 144 (although this can be increased if needed). Once the arrays are full, their data are passed to a subroutine which uses the frequency-modified Fourier transform (FMFT) method of Šidlichovský & Nesvorný (1996) to compute the orbital frequencies of the planets with the corresponding amplitudes – which for low-eccentricity orbits are approximately equal to the semimajor axes – and initial phases. The FMFT routine by Šidlichovský & Nesvorný (1996) contains a Hanning window filter that removes short-period oscillations and cleans the signal. The output is written to a file as the simulation runs.

Once the FMFT subroutine has finished the simulation carries on until the arrays are full again, the frequencies are computed again over the next interval and written to disc, and the process is repeated until the simulation ends. At the end of the simulation, there exists a file whose output contains the orbital frequencies of all the planets computed over a series of time intervals of at most 1 048 576 time-steps for each interval. One may then apply Laskar's frequency map analysis (FMA, Laskar 1993) to the data.

2.3 Application of SWIFT MVS FMA: analysis of the current system

We have simulated 1250 initial conditions of the TRAPPIST-1 system from Agol et al. (2021). For the analysis presented below we picked one system wherein the resonant angles of the outer five planets librated with low amplitude, because this is the expected outcome from a system that migrated into resonance in the presence of a gas disc (Delisle et al. 2012). A resonant chain is characterized by all the mean motions of the planets being near resonance, such that $\nu = (j + 1)n' - jn$ is a relatively slowly varying variable for each pair of planets, with a period much longer than the individual orbital periods of the planets. We find that for all the five outer resonances $\nu = -4.68006$ rad yr^{-1}. To maintain the resonance implies that the longitudes of periastrion of the five outer planets all regress with the same frequency, i.e. for these planets we expect that $\varpi = -4.68006$ rad yr^{-1}. A Fourier analysis of the vectors $e\exp(\iota\varpi)$ indicates that this is the case: the longitudes of periastron of planets d to h indeed all regress with the same frequency ν.

Table 1. Frequency decomposition of planet d. The leftmost columns show the frequencies of $e_d \exp(\imath \varpi_d)$ and the rightmost columns those of $e_d \exp[\imath(3\lambda_e - 2\lambda_d - \varpi_d)]$. The amplitude columns are essentially the values of the forced eccentricity of planet d.

Freq (rad yr^{-1})	Amplitude (10^{-3})	Freq (rad yr^{-1})	Amplitude (10^{-3})
$-4.680\,06$	$4.101\,85$	-6.5363×10^{-7}	$4.114\,97$
$0.112\,218$ (g_3)	$0.477\,816$	$-4.792\,27$ ($\nu - g_3$)	$0.482\,074$
$0.180\,291$ (g_4)	$0.389\,516$	$-4.860\,35$ ($\nu - g_4$)	$0.397\,321$
$0.168\,342$ (g_2)	$0.230\,608$	$-4.848\,41$ ($\nu - g_2$)	$0.236\,361$

However, libration of the resonant angles does not necessarily imply that the planets are in resonance. According to Delisle et al. (2012) the libration could be a geometric projection effect caused by tidal separation. One way to check this is to decompose the quantity $e\exp(\imath\phi)$, where $\phi = (j + 1)\lambda' - j\lambda - \varpi$ or $\phi = (j + 1)\lambda' - j\lambda - \varpi'$. Delisle et al. (2012) claim that in a truly resonant case $(j + 1)n' - jn \approx 0$, and thus $(j + 1)\lambda' - j\lambda$ has a long period, and the ϖ are dominated by the secular eigenmodes, which also have long periods. If the libration of the angles is a projection effect due to tidal separation, then $(j + 1)\lambda' - j\lambda$ and ϖ are dominated by short periods (high frequencies), with frequencies equal to $\nu - g$. In Table 1, we show frequency output for planet d from a set of initial conditions wherein all the resonant angles of the outer five resonances librated (see Fig. 3). It is clear from this Fourier decomposition that the current eccentricity of planet d is a purely forced eccentricity caused by its proximity to resonance with planet e. We find that the dominant terms in the decomposition of $e_d \exp[\imath(3\lambda_e - 2\lambda_d - \varpi_d)]$ have frequencies -4.792 and -4.860 rad yr^{-1}, which are equal to $\nu - g_3$ and $\nu - g_4$, respectively. For this argument the term with the largest amplitude, however, has a frequency close to zero because it is

caused by the forced eccentricity due to the resonance (Delisle et al. 2012). Similar results are obtained for the other resonant angles. Thus, for this specific set of initial conditions we used here, the planetary configuration appears to be resonant, but it is likely to be a geometric projection. This is the expected outcome of migration into a resonance with near-zero free eccentricity (Delisle et al. 2012). We have not applied such a rigorous analysis to other initial conditions from Agol et al. (2021) in part because the resonant angles do not always librate. However, we expect that from analysing these systems the conclusions will be similar.

2.4 Tidal evolution

In order to investigate the long-term effect of tidal damping in the planets on their orbits, we have evolved the TRAPPIST-1 planetary system subjected to planetary tides with the SyMBAt code (Puranam & Batygin 2018), which is based on Mercury-T (Bolmont et al. 2015). We analyse the tidal evolution of two distinct sets of initial conditions and apply dissipation in one or multiple planets within these initial conditions. The initial conditions consisted of both the current system and the $(3:2)^4$–4:3–3:2 chain; the latter initial conditions were obtained with migration in the gas disc. The parameter space for tidal dissipation in the planets is large due to the high number of planets and the potentially large range in k_2/Q per planet, where k_2 is the Love number and Q is the tidal quality factor. To keep the number of simulations reasonable we have taken a simplified approach. To keep the running time of the simulations reasonable we have fixed the value of $Q = 10^{-3}$ for each planet, while the k_2 values were taken from a best fit between the values of Earth and Mars as a function of planetary mass, which results in $k_2 = 0.29(m_p/M_\oplus)^{0.26}$. For each set of initial conditions we ran
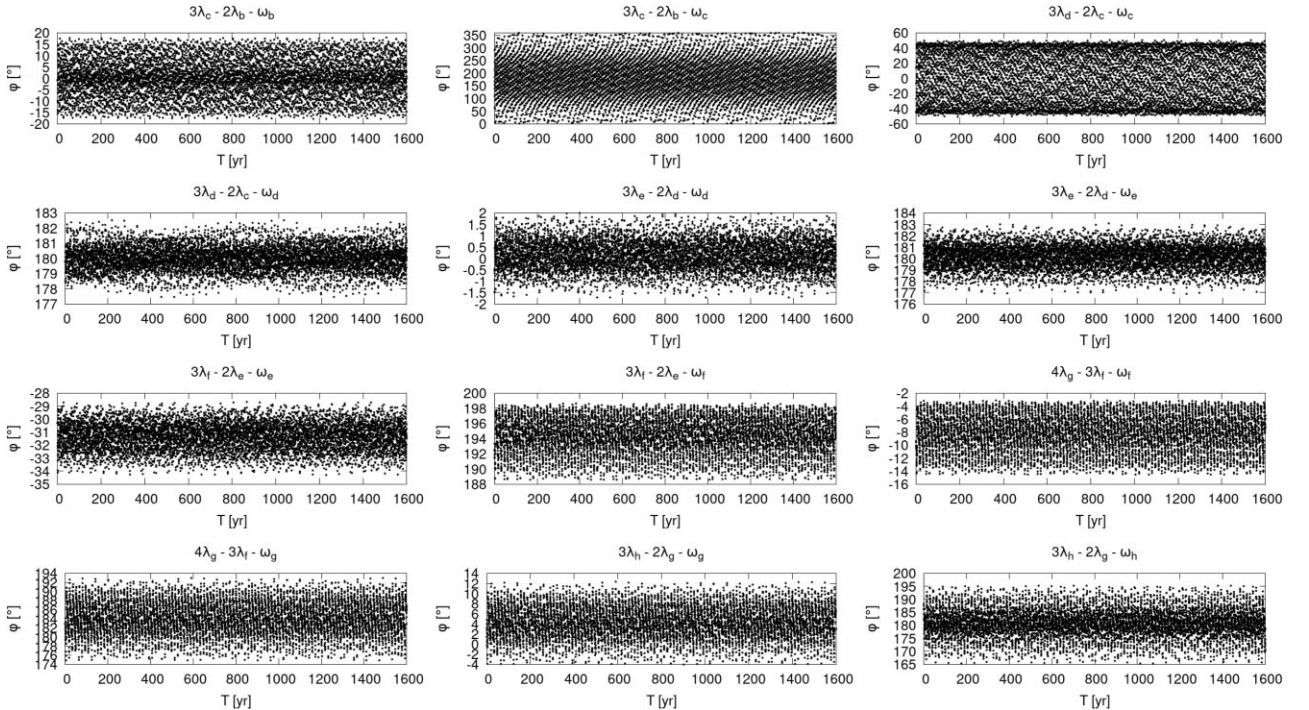
Figure 3. Evolution of resonant angles after migration through the gas phase into a $(3:2)^4$–4:3–3:2 chain. Note the different scales on the vertical axes associated to each angle. All planets are in resonance with each other, but the argument $3\lambda_c - 2\lambda_b - \varpi_c$ circulates. For this configuration $\nu = -2.640\,06$ rad yr^{-1} apart from the b-c pair for which $\nu = -29.8$ rad yr^{-1}.
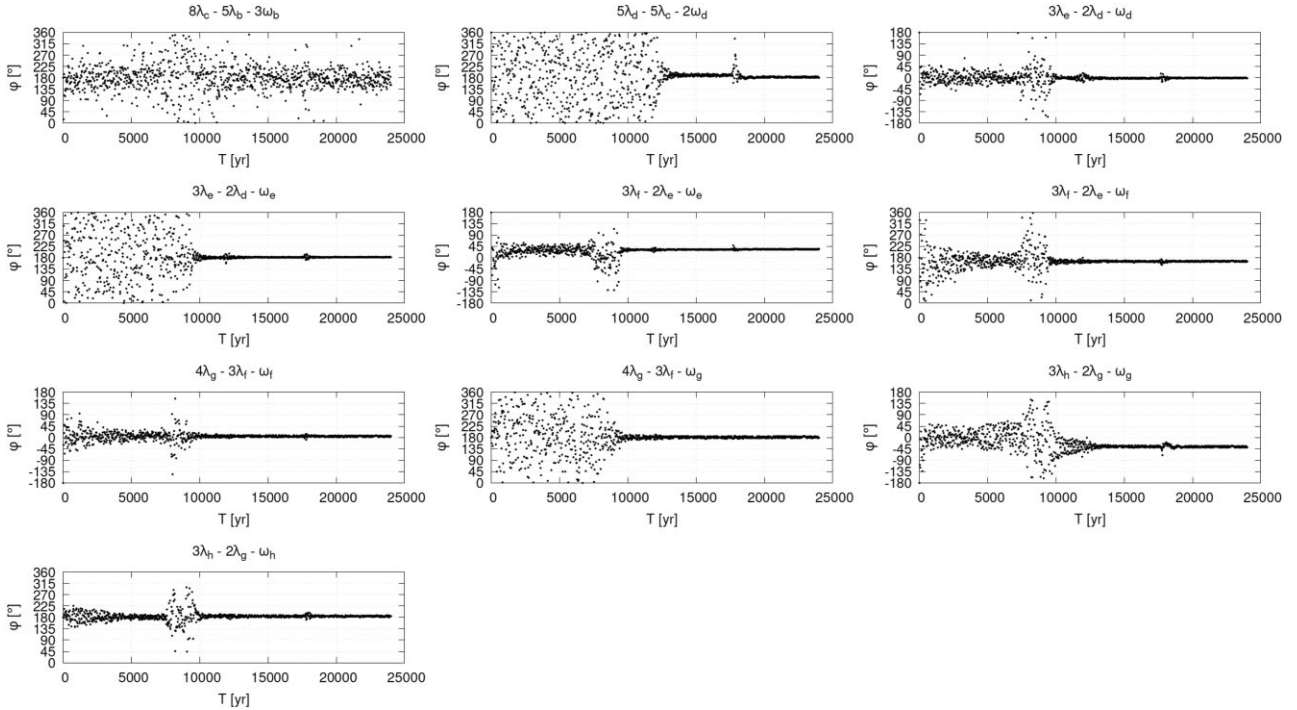
Figure 4. Resonant angle evolution during migration while attempting to reproduce the current configuration, close to a 8:5–5:3–3:2–3:2–4:3–3:2 chain. Each panel shows the evolution of a resonant angle associated with pairs of planets, for period ratios close to the observed ones. All angles are seen to be librating at the end of the simulation.

seven simulations. In the first four the damping occurred only in a single planet b to e. In the fifth to seventh simulations damping occurred in planets b and c, b to d, and b to e, respectively. Each simulation was run for 1 Myr with a time-step of 10^{-4} yr. A second set of simulations was run with $Q = 10^{-2}$ for 10 Myr to verify whether the results with $Q = 10^{-3}$ were not subjected to excessive damping.

2.5 Internal tidal models

To determine the possible interior structures of the planets, the model described by Dobos et al. (2019) was used. This model assumes an iron core, a rock mantle, a high-pressure ice polymorph layer, and either liquid water or ice I state on the surface. We set the iron core to have a mass fraction between 20 and 40 per cent of the total mass of the body, to achieve a realistic restriction on probable interior structures.

The mass, radius, and semimajor axis of the orbit are adapted from Agol et al. (2021). Their uncertainties are used in a Monte Carlo approach to generate a thousand sets of mass–radius–semimajor axis values assuming a Gaussian distribution around the mean value. For each set of parameters several interior structure models are generated, and on average we compute 16 000–25 000 solutions for each planet (a growing number from planet b to f) for a given orbital eccentricity. This provides a large range of possible solutions that preserve the most likely outcomes for the interior compositions.

Using the model of Dobos et al. (2019), the tidal heating (generated by the tidal forces from the star) is calculated for each interior structure generated. This is a viscoelastic tidal heating model with a Maxwell rheology, mimicking the effects of each layer. We assume a temperature-dependent rheology that includes the effect

of melt on viscosity and shear modulus (Henning, O'Connell & Sasselov 2009; Barr et al. 2018; Dobos et al. 2019). The k_2/Q tidal parameter is then calculated following the description of Brasser et al. (2019).

3 RESULTS

3.1 Migration in the gas disc

We implemented the disc–planet interaction prescriptions described in Section 2.1 to a seven-planet TRAPPIST-1 system. We use masses drawn from Agol et al. (2021), thus assuming that the planets have already fully formed and interact with the gaseous disc. We start each simulation with all planet pairs at period ratios 2 per cent wider than either their nominal resonant values for their currently observed 8:5–5:3–$(3:2)^2$–4:3–3:2 configuration, or the nominal resonant $(3:2)^4$–4:3–3:2 configuration. In all cases, the planets' orbits are initiated on a co-planar, circular configuration. Following the method of Tamayo et al. (2017) planet h is the only one feeling a negative torque from the disc, and it migrates inward. It is captured into the desired 3:2 resonance with planet g, and the two migrate in resonance inward towards planet f. Planet g is subsequently captured in the desired 4:3 resonance with planet f, and the process continues. This numerical set-up allows us to form both an 8:5–5:3–$(3:2)^2$–4:3–3:2 chain and a $(3:2)^4$–4:3–3:2 chain for the TRAPPIST-1 system by altering the initial positions of planets b and c between the two cases. The evolution of the resonant angle for each resonance during the migration attempting to reproduce the current resonant chain is shown in Fig. 4. The $(3:2)^4$–4:3–3:2 chain has been suggested by Huang & Ormel (2022) to be a natural outcome of type-I migration, and Teyssandier et al. (2022) show that trapping in multiple 3:2 resonances is the expected outcome, even for the b-c and c-d pairs.
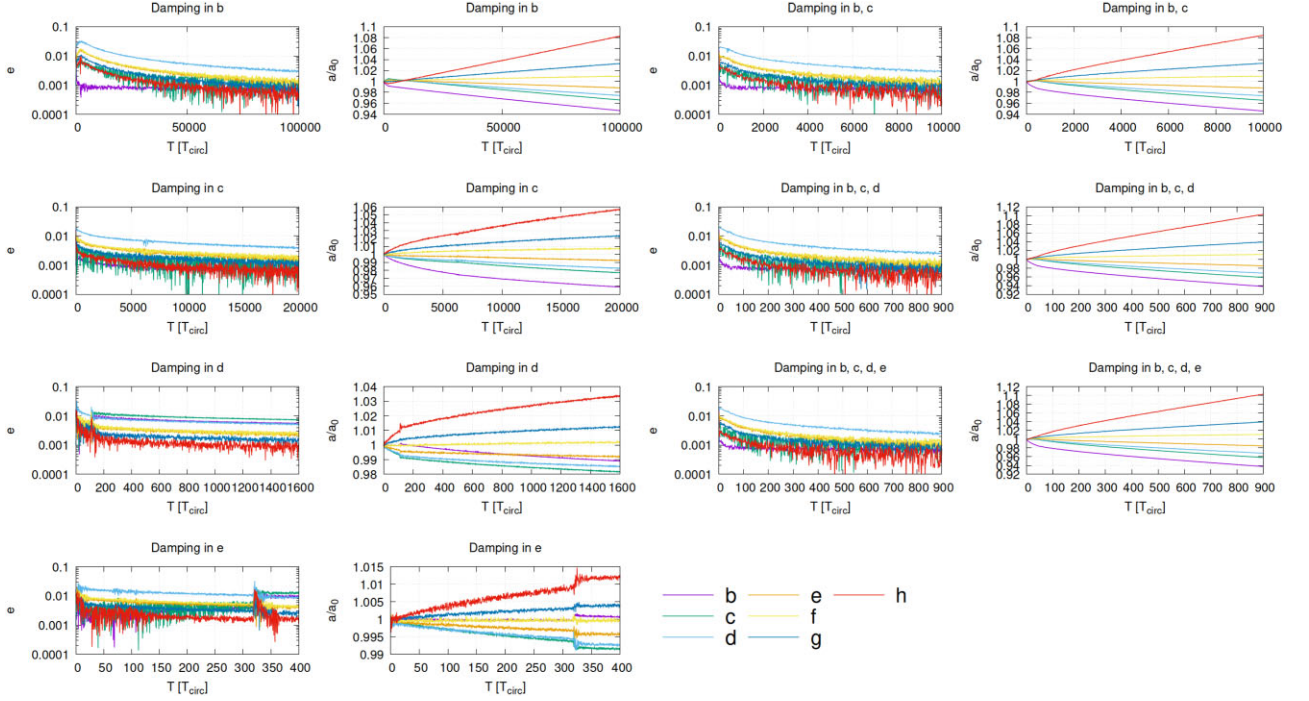
Figure 5. Tidal evolution of the current orbital configuration. The first and third columns show the eccentricities versus time while the second and fourth columns are the ratio a/a_0, where a_0 is the initial semimajor axis. Colours are purple for planet b, green for c, light blue for d, orange for e, yellow for f, deep blue for g, and red for h.

When we formed the $(3:2)^4$–4:3–3:2 chain we found that planet b was not always deeply in resonance. In order to obtain a system deeper into the resonance for planet b, we also apply artificial migration to it, but smoothly reverse the sign of the torque from negative to positive around a location close to the current observed location of the planet. In this manner, we simulate a simple planet trap (Masset et al. 2006, using the prescription from Pichierri et al. 2018).

3.2 State of the system after migration in the gas disc

The first set of initial conditions that arose from the gas-driven migration simulations attempted to reproduce the current configuration, i.e. the 8:5–5:3–$(3:2)^2$–4:3–3:2 chain. We confirm that the resonant angles of the last four resonances are librating, but not those of the inner two pairs. The frequency for the outer four resonances is found to be $\nu = -1.744\,00$ rad yr^{-1}, which is lower than the current value of $\nu = -4.680\,07$ rad yr^{-1}. This is expected because the closer the planets migrate to the exact resonance the closer the absolute frequency $|\nu|$ will be to zero. After migration the planets were closer to exact resonance so that their forced eccentricities are also higher than the current values (see Fig. 2 for how the forced eccentricity changes as a function of distance to exact resonance), and their present eccentricities are probably the result of tidal damping in the planets.

We created a second set of initial conditions where the planets were migrated into a $(3:2)^4$–4:3–3:2 chain in the presence of a gas disc because this is a likely outcome (Huang & Ormel 2022; Teyssandier et al. 2022). We have plotted all of the resonant angles of this chain at the end of the migration in Fig. 3. It is clear that apart from $3\lambda_c - 2\lambda_b - \varpi_c$ all of these angles are librating. For this particular resonant chain we computed $\nu = -2.640\,06$ rad yr^{-1}. The longitudes of periastron of planets c to e all regress with the same frequency, i.e.

for these planets $\dot\varpi = -2.640\,06$ rad yr^{-1}. An exception is planet b, for which $\dot\varpi = 1.607$ rad yr^{-1} and $\nu_{bc} = -29.809$ rad yr^{-1}. It appears as if the innermost pair of planets is not truly part of the resonant chain, and all our attempts at trying to do so have failed.
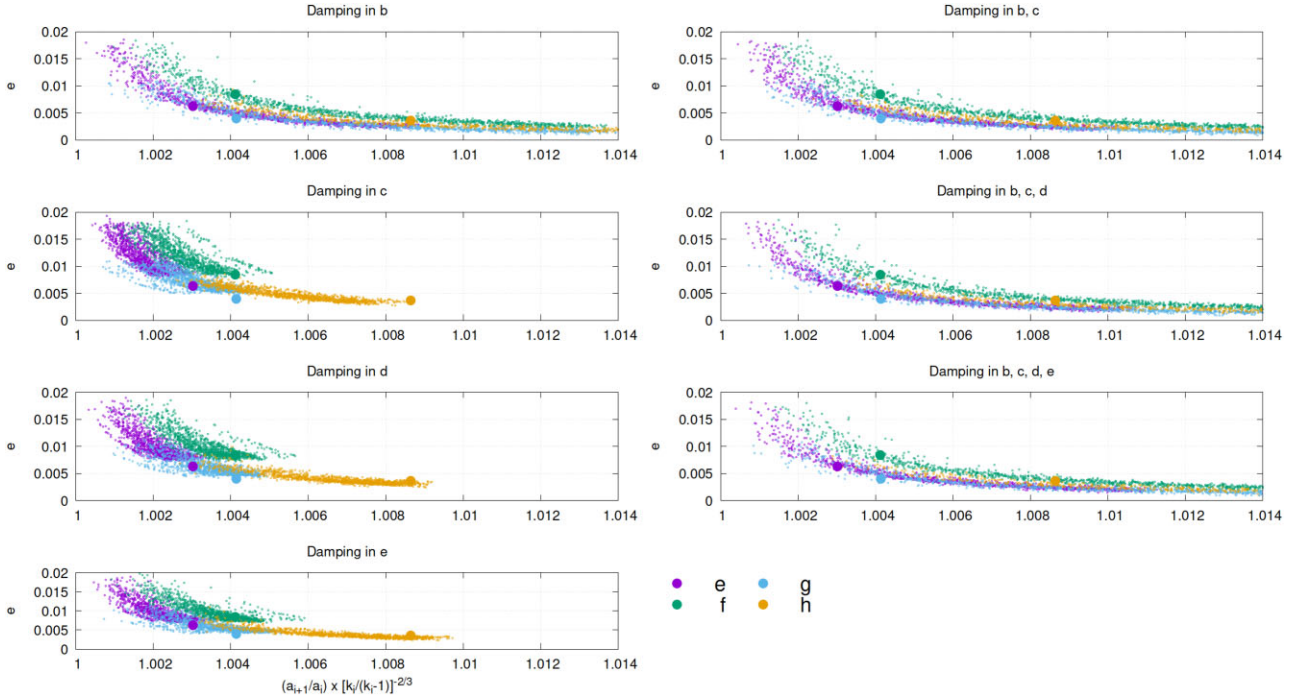
3.3 Tidal evolution of the current system

We have simulated the evolution of the resonant chain after gas-driven migration with planetary tides included using SyMBAt. The outcome of several attempts is shown in Fig. 5. The time axis is scaled to the circularization time of the planet where the damping occurs; for damping in b and c we chose the circularization time for planet c and for damping in b, c, and d and b, c, d, and e we chose the circularization time for planet d.

We show the evolution of the eccentricities (first and third columns) and the ratio a/a_0 with time (second and fourth columns) for various configurations of damping; here a_0 is the semimajor axis at the beginning of the simulation. There are two immediate visible trends.

First, the eccentricities of planets d to h damp due to dissipation in (some of) the (other) planet(s). Second, all planets separate from each other due to angular momentum conservation. The inner four planets migrate inwards while the outer three migrate outwards. The separation is clearly visible because the distance between the lines in the second and fourth columns widens as time increases. Since planets b and c are only weakly tied to the resonant chain consisting of planets d to h we see that the eccentricities of planets b and c stay low, while that of the outer five planets declines.

An alternative manner to display the tidal evolution is to make use of the equilibrium curves, as is done in Fig. 2, where we have computed the eccentricities of planets d to h versus the normalized semimajor axial ratio $(a_{i+1}/a_i) \times [(j_i + 1)/j_i]^{-2/3}$ of their resonances.

Figure 6. Tidal evolution on equilibrium curves for the current system with a five-planet resonant chain. The colours correspond to planets e–h as indicated in the legend. Large dots indicate the present configuration. The motion of the system is towards the right, i.e. towards greater separation and lower eccentricities.
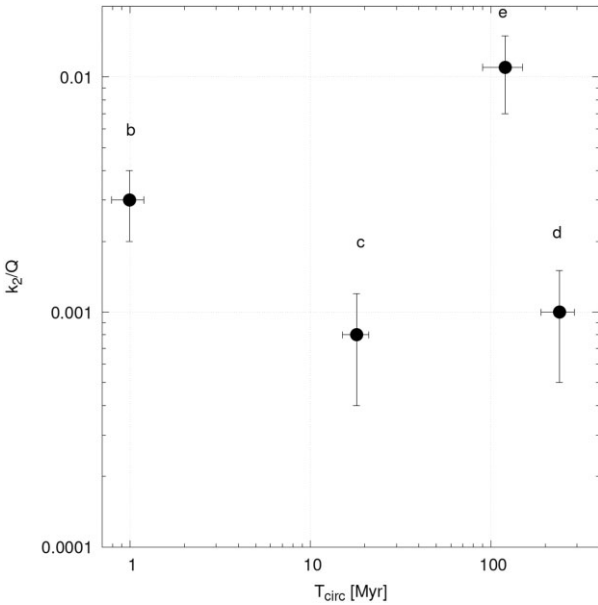
Figure 7. Long-term averaged tidal parameters for plants b to e obtained from dynamical analysis. The 1-sigma uncertainties are due to the different outcomes of the tidal simulations: different simulations result in different tidal circularization time-scales depending on which planet the damping occurs in.

As was described in the Introduction, tidal evolution will drive the planets away from resonance so that the motion in this figure is towards the bottom-right corner: the eccentricities decrease and the separation between planets increases. The big dots show the current configuration for planets e to h. It is clear that despite the age of the system the outermost pairs are still very close to resonance, with the normalized semimajor axial ratio between planets g and h being

less than 1.009, while it is less than 1.005 for the other pairs. In our simulations, the system likely started at higher eccentricity and a lower semimajor axial ratio and then was allowed to tidally evolve towards (and past) the current configuration.

One question arises from these results: Can we compute the long-term average tidal dissipation parameters of the planets from this evolution and compare them with those obtained from reasonable interior models as in Barr et al. (2018)?

Yes, it turns out that we can use the tidal evolution to compute the long-term k_2/Q for the planets assuming that the outer five migrated to their current configuration starting from an initial configuration closer to resonance (Fig. 6). Their current mutual separation cannot be overshot and thus we can compute the tidal parameters from the time it takes to reach the current configuration of the outer five planets starting from the resonant chain after migration. We proceed as follows.

We compute the time it takes in the simulation for the eccentricities of e, f, g, and h to decrease by a factor of the Euler's number, $e = 2.71828...$. We do this for each simulation wherein the damping only happens in a single planet. The tidal parameters input into the simulations yield a simulation tidal damping time-scale. From the eccentricity evolution, depending on the specific simulation and in which planet the damping occurs, we obtain the true damping time-scale in one of the planets b to e by multiplying the simulation running time with the simulation damping time-scale. The long-term value of k_2/Q is then obtained from (e.g. Batygin & Morbidelli 2013a)

$$\left(\frac{k_2}{Q}\right) = \frac{2}{21n\tau_e}\frac{m_p}{M_*}\left(\frac{a}{R_p}\right)^5,$$ (8)

where τ_e is the true eccentricity damping time-scale and R_p is the radius of the planet. The result is displayed in Fig. 7, where we plot the damping time-scale versus the long-term k_2/Q value. The
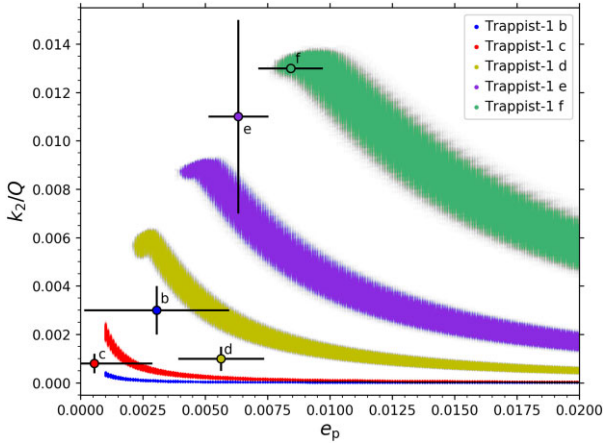
Figure 8. Tidal parameters for plants b to f obtained from interior modelling as a function of eccentricity (coloured diagonal bands). The results from the dynamical analyses are overplotted as small circles with error bars. The colour of the circles match the colours of the bands for each planet for easy comparison. Horizontal error bars: range of eccentricity values based on the work of Agol et al. (2021). Vertical error bars: possible range of the k_2/Q tidal parameter based on our dynamical simulations (see also Fig. 7).

uncertainties in both quantities are due to variations in outcome between simulations.

We compare the k_2/Q values obtained from dynamical simulations with those obtained from simulations from interior modelling as a function of eccentricity. The results of these simulations for planets b to f are shown in Fig. 8; the interior modelling simulations do not yield k_2/Q values for planets g and h because the tidal dissipation is too weak. For each orbital eccentricity value that we tested there is a range of possible k_2/Q parameters as a consequence of different possible interior structures and uncertainties in the planets' mass, radius, and semimajor axis. The results are plotted with semitransparent colours, making the less likely solutions (at the border or the ranges) appear in a shade of grey. The farther a planet is from the host star, the higher orbital eccentricity it needs to induce tidal heating in the body that is higher than heating from the star or from radioactive decay; this explains why the curves start at higher eccentricity values from planets b to f. The k_2/Q parameter monotonically decreases with orbital eccentricity because the heat flux is a constant value. Horizontal error bars show the possible eccentricity range of each planet based on the observations of Agol et al. (2021), while vertical error bars represent the results of the dynamic simulation in accordance with Fig 7. Apart from planets b and d, within uncertainty the values of k_2/Q from dynamics and interior modelling match. Considering also the current orbital eccentricities of the planets, we get the following results for the other three planets. For planet c the interior models yield $k_2/Q = (8 \pm 4) \times 10^{-4}$ with orbital eccentricity between 0.0013 and 0.0028; for planet e the two models (dynamical and interior) combined yield a value of k_2/Q in the range (0.007, 0.0092), which is narrower than that obtained only from dynamics or only based on interior modelling; and for planet f the interior models yield k_2/Q in the range (0.0114, 0.0138). Just like in Brasser et al. (2019) the tidal parameter values show some differences with the outcome from dynamics, but given the uncertainties and the number of parameters involved the near agreement is encouraging. Indeed, the agreement is better than in Brasser et al. (2019), most likely due to improved masses, radii, and eccentricities of the planets, and a corresponding narrower range of interior compositions and amount of tidal heating.

Brasser et al. (2019) suggested from dynamical simulations that for planets b and c $k_2/Q \gtrsim 2 \times 10^{-4}$ and $k_2/Q \gtrsim 10^{-3}$ respectively, while interior models with planetary mass and radii data available at that time implied k_2/Q values of a factor of a few lower. Bolmont et al. (2020) computed k_2/Q for planet e for a variety of interior models and forcing frequencies, in which they have a homogenous interior and a layered one. At the current orbital frequency of planet e their computed value of k_2/Q in the layered model is about a factor of five lower than ours derived from dynamics. For their homogenous model their derived value agrees with our interior modelling. For planet b, Huang & Ormel (2022) suggest that $Q \approx 200k_2$ from their tidal evolution simulations, so that $k_2/Q \approx 5 \times 10^{-3}$, which is close to our value obtained from dynamics, but is much higher than those obtained from the interior models.
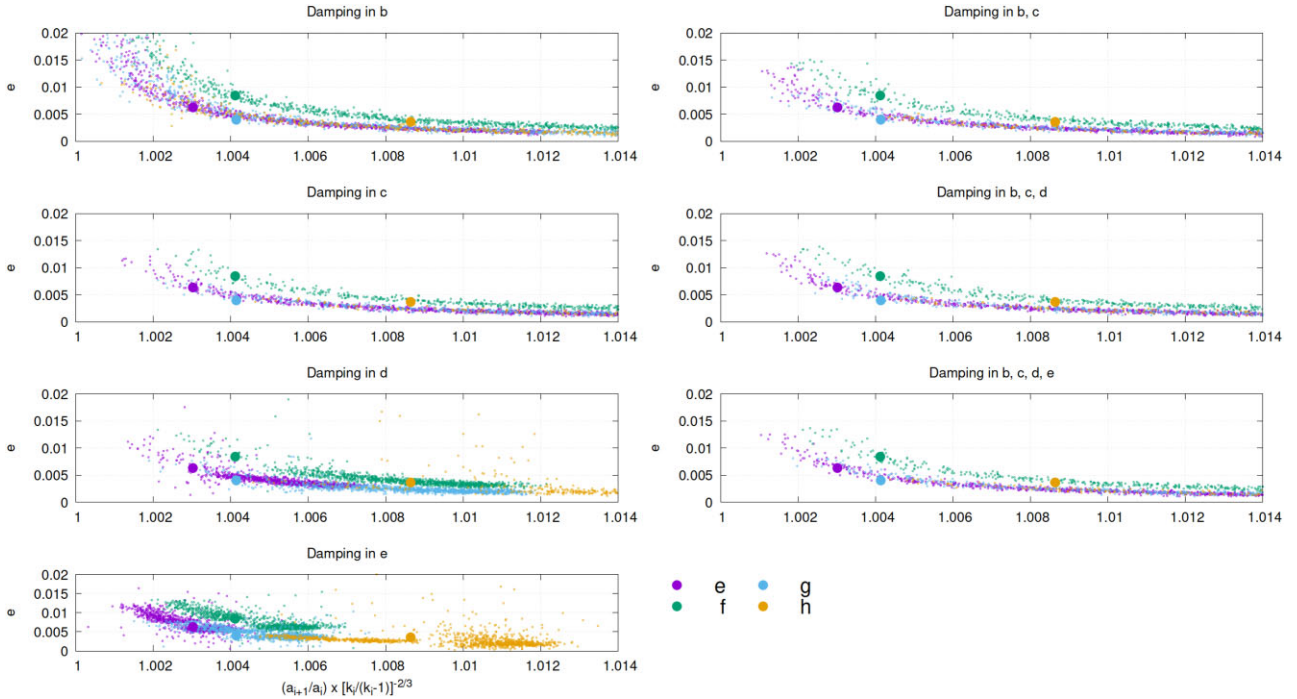
3.4 Tidal evolution of a $(3:2)^4$–4:3–3:2 chain

In this subsection we investigate whether can we reproduce the current configuration of the system from the more compact $(3:2)^4$–4:3–3:2 chain.

The tidal evolution of a $(3:2)^4$–4:3–3:2 chain is shown in Figs 9 and 10. In some cases – such as when there is only damping in planet d, in planet e, or planets b and c – the eccentricities sometimes increase before decreasing again. This is due to a pair of planets crossing a mean-motion resonance as they migrate divergently. We have found that in the cases where there is a lot of separation planets g and h cross their 5:3 resonance, while in the bottom panels (damping in planet e) planets b and c cross the 3:2 after about 70 circularization times (T_{circ}); the same happens when there is damping in planet d (third row, left-most panels) after about 30 T_{circ}. In contrast, in Fig. 5 we placed the planets closer to their current configuration and no resonances were crossed; the eccentricities of the five outer planets declined monotonically and the planets smoothly separate from each other. Fig. 10 is similar to Fig. 6.

It is clear from Figs 9 and 10 that dissipation in the planets alone does not reproduce the current configuration. Dissipation in the planets decreases the total energy, but keeps the angular momentum constant. The orbital angular momentum is given by $L = \frac{m_p}{M_*} \sqrt{a(1 - e^2)}$. After the gas-driven migration into a $(3:2)^4$–4:3–3:2 chain the fraction of the total orbital angular momentum in the planets in our simulations is 15.2, 16.4, 5.2, 11.0, 18.7, 26.2, and 7.3 per cent with the masses that we have employed. Thus, even though planet f is much farther away than planet c, it has a comparable amount of the total orbital angular momentum because the inner two planets are the most massive, and because of the weak $\sqrt{a}$ dependence on the distance (the eccentricity contribution is negligibly small). Furthermore, in the $(3:2)^4$–4:3–3:2 chain the inner four planets contain roughly half of the total orbital angular momentum. For the current configuration of the planets the fractions of the total orbital angular momentum are 14.6, 16.1, 5.3, 11.1, 19.0, 26.6, and 7.3 per cent, respectively, for the set of representative initial conditions that we have chosen; thus the fraction of the inner two planets has decreased and that of the outer five has marginally increased. To reach their current orbits from a primordial $(3:2)^4$–4:3–3:2 chain and assuming that planet d experienced almost no migration the semimajor axis of planet b had to decrease by 10 per cent and that of planet c by 7 per cent. These reductions are minimum values: if planet d is allowed to migrate then the inner two planets would have initially resided even farther away from the star and their reduction in angular momentum would be even greater. From the bottom-right panel of Fig. 9, we see that having tidal dissipation in planets b to e causes a decrease in planet b's semimajor axis of up to 6 per cent to 0.94 and in planet c's by
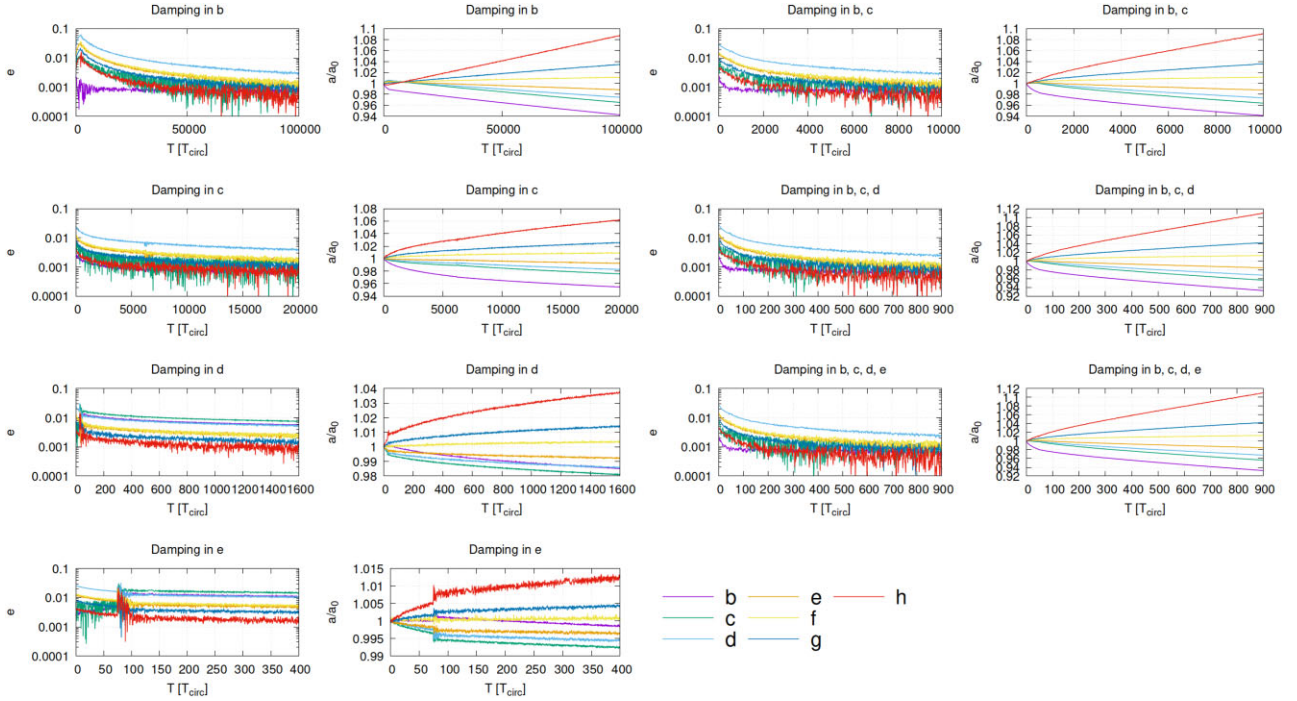
Figure 9. Tidal evolution starting from a $(3{:}2)^4$–4:3–3:2 TRAPPIST-1 chain. Different panels show the resulting evolution of the eccentricities and the relative change in semimajor axis for different choices of tidal damping. Planet b is not deeply trapped in resonance with planet c, so its eccentricity remained low.

Figure 10. Tidal evolution on equilibrium curves for a $(3{:}2)^4$–4:3–3:2 chain, showing the outer five-planet resonant chain. The colours are indicated by the legend. Large dots indicate the present configuration. The motion of the system is towards the right, i.e. towards greater separation and lower eccentricities.

up to 4 per cent to 0.96 at the end of the simulation. This results in a corresponding increase in the semimajor axis of planet h of about 10 per cent and up to 4 per cent for planet g. In contrast, planets e and f generally do not migrate much (up to 2 per cent in extreme cases). Such large amounts of outward migration amongst the outer two plan-

ets occur to compensate for the inward migration of the inner planets, but it is inconsistent with the outer planets' current period ratio and resonant configuration (see Fig. 6). The tidal motion has to occur along the equilibrium curves and thus the large amount of inward migration of the innermost planets would not only require the outer
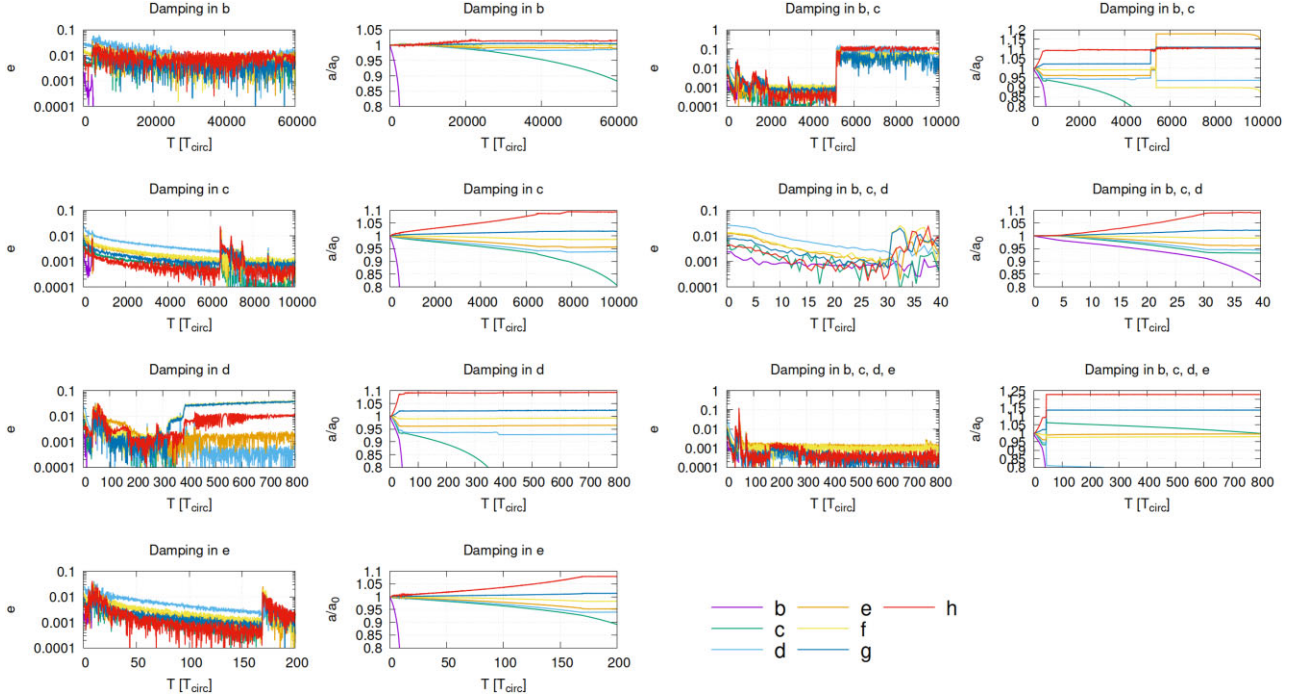
Figure 11. Tidal evolution starting with a fully resonant $(3:2)^4$–4:3–3:2 chain and with stellar tides included. The colours are indicated by the legend. Planet b rapidly detaches from the system and spirals towards the star, while eventually the same happens for planet c. The inward motion of planet c drags planet d and e with it, which causes planets f, g, and h to separate from the rest of the system.

five planets to have evolved to period ratios larger than observed, but also that their eccentricities are much lower than their current values.

The current total orbital angular momentum is about 1.3 per cent lower than in the resonant $(3:2)^4$–4:3–3:2 chain after migration. Planet b's angular momentum now is 94.8 per cent of that in the $(3:2)^4$–4:3–3:2 chain after migration, while it is 96.5 per cent for planet c assuming that we keep the position of planet d fixed. This reduction in the orbital angular momentum of these two planets equals the 1.3 per cent reduction in the total angular momentum when using the original fractions because 0.948×14.6 per cent $+ 0.965 \times 16.5$ per cent $+ 5.3$ per cent $+ 11.1$ per cent $+ 19$ per cent $+ 26.6$ per cent $+ 7.3$ per cent $= 98.7$ per cent. Since angular momentum has to be strictly conserved for tidal dissipation in the planets we deem it unlikely, if not impossible, that tidal dissipation in the planets alone has resulted in the current configuration starting from a primordial $(3:2)^4$–4:3–3:2 chain. Testing simulations with dissipation in the outer three planets will not change that outcome because the planets evolve along the equilibrium curves. Furthermore, the long-term k_2/Q values in the planets that we obtain from the tidal evolution with these initial conditions are the same as those presented in Fig. 7 within uncertainty.

The tidal parameters assumed here are may be extreme to keep simulation time short, but tests with tidal damping that is an order of magnitude weaker yields the same outcome due to the angular momentum conservation.

3.5 Inward migration of planets b and c

One manner in which the inner two planets can lose angular momentum is through tidal dissipation in the star. For a constant Q tidal model the semimajor axis evolution of the planets due to tidal

dissipation in the star is given by (e.g. Murray & Dermott 1999)

$$\frac{2}{13} a_f^{13/2} \left[1 - \left(\frac{a_0}{a_f} \right)^{13/2} \right] = -3 \left(\frac{k_2}{Q} \right)_* \left(\frac{G}{M_*} \right)^{1/2} m_p R_*^5 t_*, \quad (9)$$

where t_* is the age of the star, R_* is the stellar radius, M_* is the stellar mass, a_0 is the initial semimajor axis, and a_f is the current value. We can solve this equation for $(k_2/Q)_*$. Starting planet b in a 3:2–3:2 with planets c and d, assuming that the age of the star $t_* = 7.6 \pm 2.2$ Gyr (Burgasser & Mamajek 2017), and that the stellar radius and rotation rate have stayed the same during this whole time yields $(k_2/Q)_* = 4.2^{+1.8}_{-1.2} \times 10^{-4}$; for planet c we get $(k_2/Q)_* = 1.8^{+0.6}_{-0.4} \times 10^{-3}$, which is the same order of magnitude value. These values are much higher than that expected in solar-type stars, for which typically $(k_2/Q)_* < 10^{-7}$ (e.g. Penev et al. 2012; Ogilvie 2014). Even for lower mass stars these high values of $(k_2/Q)_*$ are not expected, even though the tidal dissipation parameter decreases before the star reaches the main sequence (Barker 2020). The uncertainties in the calculated stellar tidal parameters are mostly due to the uncertain age of the star.

However, when we add dissipation in the star into our numerical simulations starting with a $(3:2)^4$–4:3–3:2 chain we run into a few problems. An example of the evolution is displayed in Fig. 11. First, the resonance between planets c and d drags planet d with planet c as it spirals towards the star. Eventually the pair will decouple and planet d will recede from the star because it is outside the co-rotation radius. However, by this time planet b has already spiralled too far inwards to be consistent with the current configuration. Second, by the time the c-d pair decouples and planet c begins to spiral towards the star, the g-h pair has crossed the 5:3 mean motion resonance due to the near-conservation of the angular momentum due to the resonant chain and that the planets try to evolve along the equilibrium curves.

The reason that planet b decouples quickly from the system and spirals inwards is because we were unable to migrate it deep into a resonance with planet c.

We when taking into account the reduction in stellar radius with time as predicted from isochrones by Baraffe et al. (2015) we still obtain a high long-term average value of $(k_2/Q)_*$ compared to that of solar-type stars.

4 DISCUSSION

In the previous sections we argued that it is difficult to trap the planets into their current resonant configuration during an episode of gas-driven migration. Instead, the expected outcome is that the planets were caught in a chain of first-order mean-motion resonances (e.g. Ormel et al. 2017; Huang & Ormel 2022; Teyssandier et al. 2022). From such a configuration, such as a $(3:2)^4$–4:3–3:2 chain, reaching the current configuration with dissipation in the planets only seems unlikely. Yet there are a few potential caveats. For example, changing the dissipation parameters, or the strength of the dissipation in the planets relative to each other will not alter the outcome, because tidal dissipation in the planets conserves angular momentum, and the current configuration has less angular momentum than the $(3:2)^4$–4:3–3:2 chain.

Does the tidal model matter? Probably, but the differences between several models are not so great (e.g. Boue & Efroimsky 2019). At the moment we only possess one *N*-body code with a built-in tidal model, and thus we cannot test other models. However, the planets evolve along the equilibrium curves and the planetary tides conserve angular momentum. As such, we argue that changing the tidal model will not change the outcome because all tidal models conserve angular momentum; the only thing that could change is the evolution time-scale for a specific value of the tidal parameters.

Do the initial conditions matter? Yes, but starting from a different resonant configuration means a different value of the total orbital angular momentum, which stays constant during the tidal evolution in the planets alone. Therefore, the precise initial conditions are unimportant unless they are very close to the current configuration.

5 CONCLUSIONS

The TRAPPIST-1 system is lodged in a five- or possibly even seven-planet resonant chain (Luger et al. 2017; Agol et al. 2021). As a consequence of this configuration, the tidal evolution of each planet cannot be calculated individually; rather the system evolves as one unit. Due to the resonant chain the tidal evolution proceeds along a set of equilibrium curves in semimajor axis–eccentricity space wherein the planets separate from each other as their forced eccentricities are damped by dissipation in the planets while keeping the total angular momentum conserved. We show that the current 8:5–5:3–$(3:2)^2$–4:3–3:2 configuration cannot be reproduced from a primordial $(3:2)^4$–4:3–3:2 chain, so that an extra mechanism is required to decouple planets b and c from such a configuration. Dissipation in the star is one such mechanism, but with the tidal model employed here the decoupling of planet c from planet d takes longer than the time it takes for planet b to reach the star. As such it seems highly unlikely, if not impossible, to reproduce the current configuration from a $(3:2)^4$–4:3–3:2 chain using tides alone.

We also show that constraining the k_2/Q tidal parameter is possible for some of the planets using both dynamical simulations on the orbits of the planets and interior structure models. For planet c we get $k_2/Q = (8 \pm 4) \times 10^{-4}$ with orbital eccentricity between 0.0013 and 0.0028. For planet e we get a range for k_2/Q between 0.007 and 0.0092, and for planet f between 0.0114 and 0.0138. For planets b and d the values from dynamics and interior modelling do not match.

DATA AVAILABILITY

Some of the code that we use is proprietary and we have been allowed to use it and modify it with permission. As such, the simulation codes and output can be obtained upon request.

REFERENCES

Agol E. et al., 2021, Planet. Sci. J., 2, 1
Baraffe I., Homeier D., Allard F., Chabrier G., 2015, A&A, 577, A42
Barker A. J., 2020, MNRAS, 498, 2270
Barr A. C., Dobos V., Kiss L. L., 2018, A&A, 613, A37
Batygin K., Morbidelli A., 2013a, AJ, 145, 1
Batygin K., Morbidelli A., 2013b, A&A, 556, A28
Bolmont E., Breton S. N., Tobie G., Dumoulin C., Mathis S., Grasset O., 2020, A&A, 644, A165
Bolmont E., Raymond S. N., Leconte J., Hersant F., Correia A. C. M., 2015, A&A, 583, A116
Boue G., Efroimsky M., 2019, Celest. Mech. Dyn. Astron., 131, 30
Brasser R., Barr A. C., Dobos V., 2019, MNRAS, 487, 34
Burgasser A. J., Mamajek E. E., 2017, ApJ, 845, 110
Chambers J. E., 1999, MNRAS, 304, 793
Cresswell P., Nelson R. P., 2008, A&A, 482, 677
Delisle J. B., Laskar J., Correia A. C. M., Boué G., 2012, A&A, 546, A71
Dobos V., Barr A. C., Kiss L. L., 2019, A&A, 624, A2
Duncan M. J., Levison H. F., Lee M. H., 1998, AJ, 116, 2067
Elkins-Tanton L. T., Seager S., 2008, ApJ, 688, 628
Gillon M. et al., 2017, Nature, 542, 456
Goldreich P., Schlichting H. E., 2014, AJ, 147, 32
Grimm S. L. et al., 2018, A&A, 613, A68
Henning W. G., O'Connell R. J., Sasselov D. D., 2009, ApJ, 707, 1000
Henrard J., 1982, Celest. Mech., 27, 3
Huang S., Ormel C. W., 2022, MNRAS, 511, 3814
Laskar J., 1993, Celest. Mech. Dyn. Astron., 56, 191
Levison H. F., Duncan M. J., 1994, Icarus, 108, 18
Luger R. et al., 2017, Nature Astron., 1, 0129
Masset F. S., Morbidelli A., Crida A., Ferreira J., 2006, ApJ, 642, 478
Murray C. D., Dermott S. F., 1999, Solar System Dynamics. Cambridge Univ. Press, Cambridge
Ogihara M., Duncan M. J., Ida S., 2010, ApJ, 721, 1184
Ogihara M., Kokubo E., Nakano R., Suzuki T. K., 2022, A&A, 658, A184
Ogilvie G. I., 2014, ARA&A, 52, 171
Ormel C. W., Liu B., Schoonenberg D., 2017, A&A, 604, A1
Papaloizou J. C. B., Szuszkiewicz E., Terquem C., 2018, MNRAS, 476, 5032
Penev K., Jackson B., Spada F., Thom N., 2012, ApJ, 751, 96
Petrovich C., Malhotra R., Tremaine S., 2013, ApJ, 770, 24
Pichierri G., Batygin K., Morbidelli A., 2019, A&A, 625, A7

Pichierri G., Morbidelli A., Crida A., 2018, Celest. Mech. Dyn. Astron., 130, 54

Puranam A., Batygin K., 2018, AJ, 155, 157

Schoonenberg D., Liu B., Ormel C. W., Dorn C., 2019, A&A, 627, A149

Šidlichovský M., Nesvorný D., 1996, Celest. Mech. Dyn. Astron., 65, 137

Tamayo D., Rein H., Petrovich C., Murray N., 2017, ApJ, 840, L19

Tanaka H., Ward W. R., 2004, ApJ, 602, 388

Teyssandier J., Libert A. S., Agol E., 2022, A&A, 658, A170

Turbet M., Bolmont E., Ehrenreich D., Gratier P., Leconte J., Selsis F., Hara N., Lovis C., 2020, A&A, 638, A41

Unterborn C. T., Desch S. J., Hinkel N. R., Lorenzo A., 2018, Nature Astron., 2, 297

Wisdom J., Holman M., 1991, AJ, 102, 1528

This paper has been typeset from a TEX/LATEX file prepared by the author.